Two Elastodynamic Incremental Models: The Incremental Theory of Diffraction and a Huygens Method

Michel Darmon, Audrey Kamta Djakou, Samar Chehade, Catherine Potel, and Larissa Fradkin

***Abstract*— The elastodynamic geometrical theory of diffraction (GTD) has proved to be useful in ultrasonic nondestructive testing (NDT) and utilizes the so-called diffraction coefficients obtained by solving canonical problems, such as diffraction from a half-plane or an infinite wedge. Consequently, applying GTD as a ray method leads to several limitations notably when the scatterer contour cannot be locally approximated by a straight infinite line: when the contour has a singularity (for instance, at a corner of a rectangular scatterer), the GTD field is, therefore, spatially nonuniform. In particular, defects encountered in ultrasonic NDT have contours of complex shape and finite length. Incremental models represent an alternative to standard GTD in the view of overcoming its limitations. Two elastodynamic incremental models have been developed to better take into consideration the finite length and shape of the defect contour and provide a more physical representation of the edge diffracted field: the first one is an extension to elastodynamics of the incremental theory of diffraction (ITD) previously developed in electromagnetism, while the second one relies on the Huygens principle. These two methods have been tested numerically, showing that they predict a spatially continuous scattered field and their experimental validation is presented in a 3-D configuration.**

***Index Terms*— Elastodynamics, geometrical theory of diffraction (GTD), Huygens, incremental models, incremental theory of diffraction (ITD).**

I. Introduction

THE scattering of elastic waves from defects is of great interest in ultrasonic nondestructive testing (NDT). The geometrical theory of diffraction (GTD) is a classical method used for modeling diffraction from cracks, which behave locally as half-planes or infinite wedges [1], [2]. It is a high-frequency ray method, which in addition to incident and reflected rays, that introduces diffracted rays and describes the diffracted field they carry using the diffraction coefficients calculated for half-planes or infinite wedges, respectively. In other words, GTD relies on the locality principle of high frequency phenomena, which stipulates that if the vicinity of each diffraction point along the obstacle contour can be described, may be approximately, by an infinite tangent half-plane or by an infinite planar wedge, then the diffracted field radiated by this point can be described using the corresponding GTD diffraction coefficients. However, in ultrasonic NDT, it is not uncommon to encounter a diffracting edge of a flaw that cannot be approximated, even locally, by a straight line or planar wedge as shown in Figs. 3(a) and 4(a). GTD produces a discontinuity at the shadow boundaries emanating from the edge endpoints (for instance, a corner of a rectangular defect) since the GTD field is null out of the diffraction cone. GTD has other drawbacks of ray tracing: searching for the diffraction point for each observation point is not so straightforward in the complex 3-D configurations, and the GTD invalidity at caustics requires a uniform correction using special functions [3].

Incremental methods have been developed, originally in electromagnetism, to overcome these GTD limitations: incremental theory of diffraction (ITD) [4]–[6], incremental length diffraction coefficient (ILDC) [7], and equivalent edge currents (EECs) [8]. Unlike GTD, incremental methods do not require ray tracing. They treat points of the diffracting edge as fictitious sources of the field called incremental field, and the scattered field at an observation point is calculated as the sum of these incremental contributions. Incremental models provide an extension for observation angles outside of the diffraction cone and a natural uniform representation of the scattered field at caustics [4] or at the shadow boundaries emanating from edge endpoints. Incremental methods are particularly useful to better take into account the finite length and shape of a defect contour. To model diffraction from an edge of finite size, ITD can be based on GTD or [5] uniform theory of diffraction (UTD) [9], UTD being a GTD uniform correction, valid inside penumbras of incident or reflected rays and outside [9].

As in ultrasonic NDT, a crack is usually not more than a few centimeters long [10], and inspections are carried out at high frequency (1–10 MHz). GTD can be utilized, because cracks are usually large compared to the corresponding wavelengths. But GTD is theoretically valid for an infinite edge and modeling has to take into account the crack's finite extent.

This paper aims at developing elastodynamic incremental models for isotropic solids, with application to ultrasonic NDT.

Manuscript received February 11, 2019; accepted March 7, 2019. Date of publication March 12, 2019; date of current version April 24, 2019. *(Corresponding author: Michel Darmon.)*

M. Darmon and S. Chehade are with CEA-LIST, Department of Imaging and Simulation for Nondestructive Testing, 91191 Gif-sur-Yvette, France, and also with the Ecole Doctorale EOBE, University Paris-Saclay, Île-de-France, France (e-mail: michel.darmon@cea.fr; samar.chehade@cea.fr).

A. Kamta Djakou is with CEA-LIST, 91191 Gif-sur-Yvette, France (e-mail: noelleaudrey@gmail.com).

C. Potel is with Fédération Acoustique du Nord Ouest (FANO), CNRS 3110, France, and also with the Laboratoire d'Acoustique de l'Université du Maine (LAUM), UMR CNRS 6613, 72085 Le Mans, France (e-mail: catherine.potel@univ-lemans.fr).

L. Fradkin is with Sound Mathematics Ltd., Cambridge CB4 2AS, U.K. (e-mail: l.fradkin@soundmathematics.com).

Digital Object Identifier 10.1109/TUFFC.2019.2904334

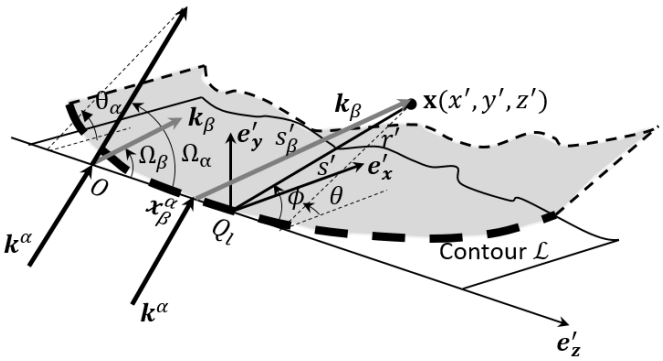

Fig. 1. Plane wave with the propagation vector $k^{\boldsymbol{\alpha}}$ incident on a stress-free crack (in gray) of contour L. Thick black arrow: direction of the incident wave and thick gray arrow: direction of the wave scattered by the half-plane tangent to the crack at the diffraction point Q_l.

An elastodynamic incremental model was developed before for an elliptical crack [11]: it is based on a Kirchhoff approximation integral on a line and will consequently necessarily predict erroneous amplitudes of edge diffracted fields; that is why the elastodynamic Kirchhoff prediction has been improved using the physical theory of diffraction (PTD) [12], especially for shear waves [12].

The methods proposed in this paper are more effective than this Kirchhoff-based method [11] since they rely on GTD or PTD which is a much better recipe than Kirchhoff for modeling edge diffraction. In Section II, an elastodynamic ITD is developed using the standard approach previously developed in electromagnetism [4]. A new elastodynamic incremental model based on the Huygens principle is also proposed. Section III describes the numerical and experimental validations of both models. Section IV provides the conclusion.

II. Incremental Models

Let us consider a curved stress-free crack of contour L embedded in an elastic homogeneous and isotropic space. Let the crack be irradiated by a plane wave (Fig. 1)

$$\mathbf{u}^{\boldsymbol{\alpha}}(\mathbf{x}) = A\mathbf{d}^\alpha e^{i(-\omega t + \mathbf{k}^\alpha \cdot \mathbf{x})} \tag{1}$$

where the superscript α = L, TV, or TH (longitudinal, transverse vertical, or transverse horizontal) is used to denote the incident wave mode, A is the wave amplitude, $\mathbf{d}^\alpha$ its polarization (unit vector in the direction of particle motion), $\mathbf{k}^\alpha$ its wave vector whose magnitude is noted $k_\alpha = \omega/c_\alpha$, with ω being the circular frequency, c_α being the speed of the corresponding mode, i being the imaginary unit, t is the time, and $\mathbf{x}$ is the observation point. Below the exponential factor $\exp(-i\omega t)$ is implied but omitted everywhere.

Incremental methods assume that points Q_l of the diffracting edge are all fictitious Huygens sources of a field defined as the incremental field $\boldsymbol{F}_\beta(Q_l, \mathbf{x})$. Then, at an observation point $\mathbf{x}$, the field $\boldsymbol{v}_\beta$ diffracted by the contour L is the integral over the contour L of the incremental field

$$\boldsymbol{v}^\alpha_\beta(\mathbf{x}) = \int_L \boldsymbol{F}_\beta(Q_l, \mathbf{x}) e^{ik_\alpha l \cos\Omega_\alpha(l)} dl \tag{2}$$

with dl being the edge increment. We have developed two different methods to determine this incremental field in elastodynamics: one based on the GTD locality principle (ITD) and one based on the Huygens principle.

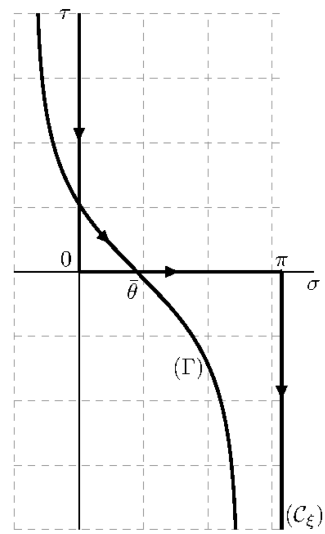

Fig. 2. Integration contours Γ and C_ξ in the complex plane $\sigma + i\tau$.

A. Elastodynamic Incremental Theory of Diffraction

At the diffraction point Q_l, let the crack edge be approximated by a half-plane tangent to the edge at this diffraction point (see Fig. 1). Let Q_l be the origin of the local Cartesian coordinate system $\{\mathbf{e}'_x, \mathbf{e}'_y, \mathbf{e}'_z\}$ associated with this half-plane. It is convenient to express the incident wave vector $\mathbf{k}^{\boldsymbol{\alpha}} = k_\alpha \cdot (\sin\Omega_\alpha \cos\theta_\alpha, \sin\Omega_\alpha \sin\theta_\alpha, \cos\Omega_\alpha)$ in the associated spherical coordinates $(k_\alpha, \Omega_\alpha, \theta_\alpha)$ and the observation point $\mathbf{x}$, using either the local Cartesian coordinates (x', y', z') or another set of associated local spherical coordinates (s', ϕ, θ).

The exact scattered field $\boldsymbol{u}^\alpha_\beta(\mathbf{x}, \Omega_\alpha, \theta_\alpha)$ generated by a plane elastic wave irradiating a half-plane can be described using the plane-wave spectral decomposition [2]

$$\boldsymbol{u}^\alpha_\beta(\mathbf{x}, \Omega_\alpha, \theta_\alpha) = i\frac{q_\beta \kappa_\beta}{2\pi} \int_\Gamma \Psi_\beta(\lambda, \Omega_\alpha, \theta_\alpha) \sin\lambda \boldsymbol{d}_{\boldsymbol{\beta}}(\Omega_\beta, \theta) \times e^{ik_\beta[r' \sin\Omega_\beta \cos(\lambda - \bar{\theta}) + z' \cos\Omega_\beta]} d\lambda \tag{3}$$

with β being the scattered wave mode, $q_\beta = k_\beta \sin\Omega_\beta$ and $\kappa_\beta = c_L/c_\beta$ the dimensionless slowness of the scattered wave

$$\Psi_\beta(-q_\beta \cos\lambda, \mathrm{sgn}(\sin\theta)) = \frac{g_\beta(-q_\beta \cos\lambda, \mathrm{sgn}(\sin\theta))}{q_\alpha \cos\theta_\alpha - q_\beta \cos\lambda} \tag{4}$$

where expressions of g_β are given from [2] in [13, Appendix B] and $\bar{\theta}$ given by

$$\begin{cases} \bar{\theta} = \theta, & \text{if } \theta \le \pi\,(y' \ge 0) \\ \bar{\theta} = 2\pi - \theta, & \text{if } \theta > \pi\,(y' < 0). \end{cases} \tag{5}$$

$\boldsymbol{d}_{\boldsymbol{\beta}}$ is the polarization vector of the scattered wave, and Γ is the steepest descent contour shown in Fig. 2. The diffraction angle Ω_β is related to the incidence angle Ω_α by the law of edge diffraction

$$k_\beta \cos\Omega_\beta = k_\alpha \cos\Omega_\alpha. \tag{6}$$

An asymptotic evaluation of (3) which utilizes the steepest descent method leads to the GTD diffracted field [2]

$$\boldsymbol{u}_\beta^\alpha(\mathbf{x}, \Omega_\alpha, \theta_\alpha) = u^\alpha\left(\mathbf{x}_\beta^\alpha\right) \frac{e^{ik_\beta s'_\beta}}{\sqrt{k_\beta s'_\beta}} D_\beta^\alpha(\Omega_\alpha, \theta_\alpha, \theta) \boldsymbol{d}_{\boldsymbol{\beta}}(\Omega_\beta, \theta) \quad (7)$$

with the diffraction coefficient

$$D_\beta^\alpha(\Omega_\alpha, \theta_\alpha, \theta) = \frac{e^{i\frac{\pi}{4}}}{\sqrt{2\pi}} k_\beta^2 \Psi_\beta(\bar{\theta}, \Omega_\alpha, \theta_\alpha) |\sin\theta| \quad (8)$$

with $s'_\beta = r'/\sin\Omega_\beta$, $r' = (x'^2 + y'^2)^{1/2}$, and $\mathbf{x}_\beta^\alpha = (0, 0, z' - s'_\beta \cos\Omega_\beta)$ being the diffraction point on the diffracting edge (the single ray satisfying the law of edge diffraction and reaching $\mathbf{x}$ emanates from $\mathbf{x}_\beta^\alpha$) and $\boldsymbol{u}^{\boldsymbol{\alpha}}(\mathbf{x}_{\boldsymbol{\beta}}^{\boldsymbol{\alpha}}) = u^\alpha(x_\beta^\alpha) \cdot \mathbf{d}^\alpha$.

Implementing the procedure described in [4], the incremental field $\boldsymbol{F}_\beta(Q_l, \mathbf{x})$ is the field $\boldsymbol{F}_\beta(z' = 0, \mathbf{x})$ radiated by the diffraction point Q_l treated as lying on the edge of the tangential half-plane.

It is then assumed that the field diffracted by a half-plane edge is the sum of incremental fields emitted by all diffraction points along the infinite edge

$$\boldsymbol{u}_\beta^\alpha(\mathbf{x}, \Omega_\alpha, \theta_\alpha) = \int_{-\infty}^{+\infty} \boldsymbol{F}_\beta(z', \mathbf{x}) e^{ik_\alpha z' \cos\Omega_\alpha} dz'. \quad (9)$$

Using notation $\xi = \Omega_\alpha$, the inverse Fourier transform gives

$$\boldsymbol{F}_\beta(z', \mathbf{x}) = \frac{k_\alpha}{2\pi} \int_{C_\xi} \boldsymbol{u}_\beta^\alpha(\mathbf{x}, \xi, \theta_\alpha) \sin\xi e^{-ik_\alpha z' \cos\xi} d\xi. \quad (10)$$

The contour C_ξ in the $\xi = \sigma + i\tau$ plane is shown in Fig. 2. Thus, at any arbitrary observation point, the incremental contribution from Q_l to the diffracted field is

$$\begin{aligned} \boldsymbol{F}_\beta(Q_l, \mathbf{x}) &= \boldsymbol{F}_\beta(z' = 0, \mathbf{x}) \\ &= \frac{k_\alpha}{2\pi} u^\alpha(Q_l) \int_{C_\xi} \boldsymbol{u}_\beta^\alpha(\mathbf{x}, \xi, \theta_\alpha) \sin\xi d\xi. \end{aligned} \quad (11)$$

Note that the incident field in this local Cartesian coordinate is $u^\alpha(Q_l) = 1$ and is, therefore, independent of ξ and thus can be taken outside the integral sign. Replacing $\boldsymbol{u}_\beta^\alpha(\mathbf{x}, \xi, \theta_\alpha)$ in (11) by its (3), the incremental field $\boldsymbol{F}_\beta(Q_l, \mathbf{x})$ becomes

$$\begin{aligned} \boldsymbol{F}_\beta(Q_l, \mathbf{x}) = i \frac{\kappa_\beta k_\alpha}{4\pi^2} u^\alpha(Q_l) \times \int_{C_\xi} \int_\Gamma q_\beta(\xi) \Psi_\beta(\lambda, \xi, \theta_\alpha) \\ \times \sin\lambda \sin\xi \boldsymbol{d}_{\boldsymbol{\beta}}(\xi, \lambda) e^{ig(\lambda, \xi)} d\lambda d\xi \end{aligned} \quad (12)$$

with $g(\lambda, \xi) = k_\beta[r' \sin\Omega_\beta(\xi) \cos(\lambda - \bar{\theta}) + z' \cos\Omega_\beta(\xi)]$. Angle Ω_β is related to ξ by the law of edge diffraction $k_\beta \cos\Omega_\beta(\boldsymbol{\xi}) = k_\alpha \cos\boldsymbol{\xi}$. Therefore, the phase function in (12) can be written as

$$g(\lambda, \xi) = s'\left[\sin\phi \cos\left(k_\beta^2 - k_\alpha^2 \cos^2\xi\right)^{1/2} + k_\alpha \cos\phi \cos\xi\right] \quad (13)$$

with s' being the distance between the observation point and the diffraction point Q_l. Integral (12) has two stationary phase points

$$(\lambda_0, \xi_0) = \left(\bar{\theta}, \arccos\left(\frac{k_\beta}{k_\alpha} \cos\phi\right)\right) \quad \text{and } (\bar{\theta}, 0). \quad (14)$$

The second phase stationary point corresponds to grazing incidence. In this paper, we study the contribution of the first stationary phase point alone. The obtained results are, therefore, not valid for any grazing incidence. Applying the steepest descent method to the double integral (12) leads to the following high-frequency approximation of the incremental field (see the Appendix or [13] for details)

$$\boldsymbol{F}_\beta(Q_l, \mathbf{x}) = \frac{1}{\sqrt{2\pi i}} \sin\phi D_\beta^\alpha(\Omega_\alpha(\phi), \theta_\alpha, \theta) \boldsymbol{d}_{\boldsymbol{\beta}}(\phi, \theta) \frac{e^{ik_\beta s'}}{s'} \quad (15)$$

with

$$\Omega_\alpha(\phi) = \arccos\left(\frac{k_\beta}{k_\alpha} \cos\phi\right). \quad (16)$$

This asymptote of the incremental field, which is valid in the far field zone $k_\beta s' \gg 1$, is a spherical wave weighted by a scattering coefficient. Thus, each point on the defect contour points acts as a fictitious source of the spherical wave.

Note that if the contour L is a straight line (the crack is a half-plane), then substituting (15) into (2), the diffracted field is

$$\begin{aligned} \boldsymbol{v}_\beta^\alpha(\mathbf{x}) = \int_{-\infty}^{\infty} u^\alpha(Q_l) \frac{\sin\phi(l)}{\sqrt{2\pi i}} D_\beta^\alpha(\Omega_\alpha(\phi(l)), \theta_\alpha, \theta) \\ \times \frac{e^{ik_\beta s'}}{s'} \boldsymbol{d}_{\boldsymbol{\beta}}(\phi, \theta) dl. \end{aligned} \quad (17)$$

In the global Cartesian coordinate system $\{O, \mathbf{e}_x = e'_x, \mathbf{e}_y = e'_y, \mathbf{e}_z = e'_z\}$, the diffraction point is $Q_l(0, 0, l)$. The corresponding phase stationary point l_s is the z-coordinate of the diffraction point on the contour. At this stationary point, $\phi(l_s) = \Omega_\beta$, $s'(l_s) = s'_\beta$, and the phase stationary point contribution to (17) is

$$\boldsymbol{v}_\beta^\alpha(\mathbf{x}) = e^{ik_\alpha l_s \cos\Omega_\alpha} D_\beta^\alpha(\Omega_\alpha, \theta_\alpha, \theta) \boldsymbol{d}_{\boldsymbol{\beta}}(\Omega_\beta, \theta) \frac{e^{ik_\beta s'_\beta}}{\sqrt{k_\beta s'_\beta}}. \quad (18)$$

ITD gives, thus, the GTD solution (7) for infinite straight edges.

B. Huygens Method

According to Huygens, when impacted by an incident plane wave, each point on an obstacle serves as the source of a spherical secondary wavelet with the same frequency as the primary wave. The amplitude at any point is the superposition of these wavelets. This theory gives a simple qualitative description of diffraction but needs to be adapted to provide a good agreement with more exact scattering formulations (such as GTD). Therefore, in our Huygens method, we postulate an ansatz, in which the amplitude of the scattered field at an observation point is obtained by integrating the spherical waves' contributions from the points along the edge and by weighting each contribution by a directivity factor (henceforth named K)

$$\boldsymbol{v}_\beta^\alpha(\mathbf{x}) = \int_L \boldsymbol{K} u^\alpha(Q_l) \frac{e^{ik_\beta s'}}{s'} dl \quad (19)$$

where L is the crack contour, and dl is the length of an elementary arc along the contour L. To determine the unknown $\boldsymbol{K}$ vector in (19), we again use Huygens' principle: the latter tells us that the scattered wavefront from an infinite

straight edge is the envelope of the secondary spherical waves and is, thus, cylindrical or conical in the field far from the flaw as predicted by GTD. To mathematically transform the sum of spherical waves of our Huygens proposed integral into a cylindrical or conical waveform, we apply below the stationary phase method to Huygens' integral for a straight infinite edge and the obtained far-field approximation is identified to the GTD one to fix the K coefficient.

If the contour L is a straight segment with ends a and b, the angles of incidence Ω_α and θ_α are the same at any discretization points on the diffracting edge. In the frame $\{O, \boldsymbol{e}_x, \boldsymbol{e}_y, \boldsymbol{e}_z\}$, the distance between the diffraction point $Q_l = (0, 0, l)$ on the contour L and an observation point $\mathbf{x} = (x, y, z) = (x', y', z' + l)$ is $s' = [(z - l)^2 + r'^2]^{1/2}$ with $r' = (x'^2 + y'^2)^{1/2}$. Using the law of edge diffraction (6), the phase function of diffracted field (19) can be written as

$$q(l) = \sqrt{(z - l)^2 + r'^2} + l \cos \Omega_\beta \tag{20}$$

The stationary phase point is the edge diffraction point $(0, 0, l_s)$ with

$$l_s = z - \frac{r'}{\tan \Omega_\beta}. \tag{21}$$

Therefore, in the far field ($k_\beta r' \gg 1$), the diffracted field (19) can be approximated by the phase stationary method

$$\boldsymbol{v}_\beta^\alpha(\mathbf{x}) = H(l_s - a) H(b - l_s) A \boldsymbol{K} e^{i\frac{\pi}{4}} \frac{\sqrt{2\pi}}{\sin \Omega_\beta} \frac{e^{i(k_\alpha l_s \cos \Omega_\alpha + k_\beta s'_\beta)}}{\sqrt{k_\beta s'_\beta}} \tag{22}$$

when the phase stationary point is far from the edge extremities a and b, and H is the Heaviside function. The coefficients vector K can be chosen to be

$$\boldsymbol{K} = \frac{\sin \Omega_\beta}{\sqrt{2i\pi}} D_\beta^\alpha(\Omega_\alpha, \theta_\alpha, \theta) \boldsymbol{d}_\beta(\Omega_\beta, \theta) \tag{23}$$

so that for an infinite straight edge ($a \to -\infty$, $b \to \infty$), the stationary point contribution gives the GTD diffracted field (7).

The formulation of Huygens method (19) has similitudes with (45) of the paper [11]. But this cited equation was simply a step of calculation in [11] and led to no modeling application. Moreover, this equation has been established only for an elliptic crack and compressional waves. In contrast, the Huygens method proposed here can be applied for any crack shape and also for shear waves.

Finally, incremental fields in the ITD and Huygens models can both be represented using the K function by

$$\boldsymbol{F}_\beta(Q_l, x)|_{\text{ITD}} = \frac{e^{ik_\beta s'}}{s'} K(\Phi(l)) \tag{24}$$

$$\boldsymbol{F}_\beta(Q_l, x)|_{\text{Huygens}} = \frac{e^{ik_\beta s'}}{s'} K(\Omega_\beta) \tag{25}$$

with

$$\boldsymbol{K}(\zeta) = \frac{\sin \zeta}{\sqrt{2\pi i}} D_\beta^\alpha(\Omega_\alpha(\zeta), \theta_\alpha, \theta) \boldsymbol{d}_\beta(\zeta, \theta). \tag{26}$$

The Huygens formula (25) differs from the ITD formula (24) by the argument ζ of the coefficient $K(\zeta)$. In ITD, ζ is the angle ϕ characterizing the ray issuing from an arbitrary discretization point to the observation point, whereas in the Huygens method, it is the diffraction angle Ω_β. Consequently, ITD is parametrized by the local angle ϕ, whereas the Huygens method is parametrized by the incident angle Ω_α according to (6). Both methods add endpoints contributions to the classical edge contribution. Even if endpoints probably radiate differently from other points inside the edge segment, the ITD and Huygens models lead to a more physical description than GTD one's [see Figs. 3(a) and 4(a)].

III. Results

A. Implementation

For both Huygens and ITD models, the diffracted field is then computed using (2) [and (24)–(26) for ITD, (25) and (26) for Huygens], where the integration along the edge L is approached numerically by a discrete sum. For the case studied here of an incident plane wave, the GTD diffraction coefficient and scattered polarization are the same for all meshed edge points for Huygens computations [see (25)], whereas they vary along the edge for ITD [see (24) depending on $\Phi(l)$]. Huygens is consequently much less time-consuming than ITD.

B. Numerical Tests

The ITD and Huygens models have been subjected to two different kinds of numerical tests. In both tests, the longitudinal/transversal speeds and frequency of the incident wave are, respectively, $c_L = 5900$ (m/s) and $c_T = 3230$ m/s and 1 MHz.

The first test is a comparison to GTD. The numerical tests involve here a longitudinal oblique ($\Omega_{\alpha=L} = 60°$ and $\theta_{\alpha=L} = 60°$) incident wave and both longitudinal (Fig. 3) and transversal (Fig. 4) diffracted waves from a finite straight edge. The frame center O is taken as the center of a 40-mm-long crack edge. The observation points are chosen to lie in the plane (e'_y, e'_z) normal to the crack plane and containing the crack edge (see Fig. 1): $\theta = 90°$ or $\theta = 270°$. There is no shadow boundary of the incident or reflected fields (divergence of the GTD diffraction coefficient) in this observation plane since, for example, for P scattered waves, $\theta \neq \theta_\alpha$ and $\theta \neq 2\pi - \theta_\alpha$.

GTD is a ray method. Given an observation point, the diffraction point on the edge can be found, which gives rise to a diffracted ray satisfying the law of edge diffraction and reaching this observation point. The diffracted field amplitude is then evaluated using the GTD formula (7). The classical GTD produces a discontinuity at the shadow boundaries emanating from the edge endpoints [see Figs. 3(a) and 4(a)]. Unlike GTD, the Huygens model involves summing up the wavelets generated by the fictitious sources on the edge. Therefore, in this model (and also in ITD), the edge endpoints contribute to the diffracted field, making it continuous [see Figs. 3(b) and 4(b)]. Since GTD is discontinuous at the shadow boundary of the edge endpoints, but Huygens (or ITD) is continuous, the difference between GTD and Huygens (or ITD) solutions [see Fig. 3(d)] is discontinuous and behaves as a sign function. The appearance of the sign function can be mathematically shown by calculating the asymptotic uniform contribution of

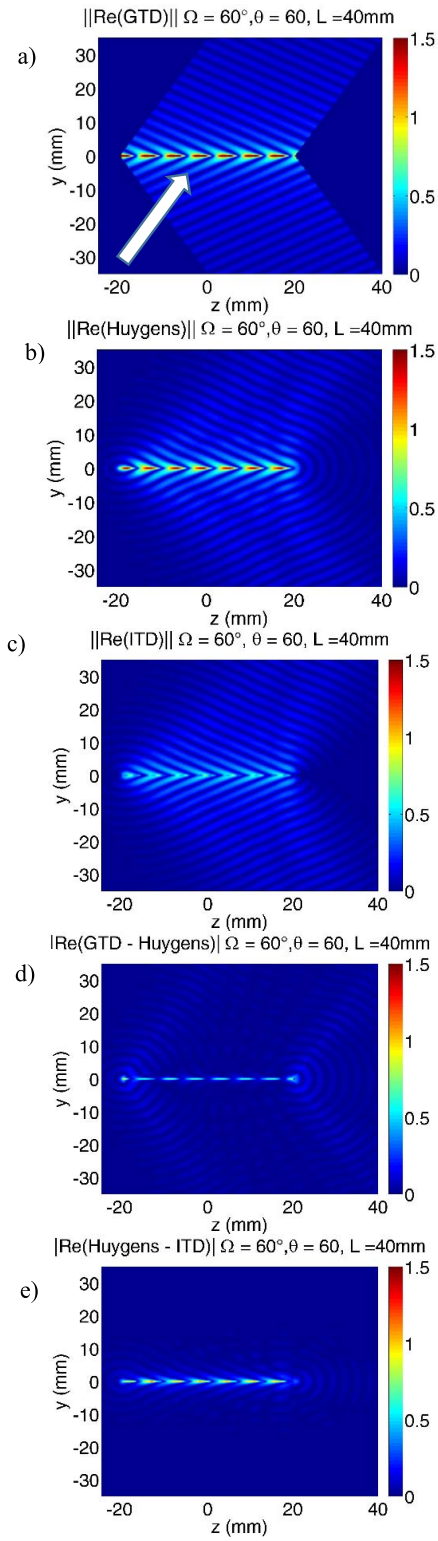

Fig. 3. Diffraction of an oblique incident longitudinal wave (white arrow, $\Omega_\alpha = 60°$ and $\theta_{\alpha=L} = 60°$) by a planar 40-mm-long crack, observed in the plane normal to the crack and containing the crack edge. Results for the longitudinal diffracted wave, normalized by the incident amplitude: real parts of (a) GTD, (b) Huygens, and (c) ITD solutions. Absolute difference between real parts of (d) Huygens and GTD solutions and (e) Huygens and ITD solutions.

coalescing extremity points and stationary phase points in the Huygens' integral using a method proposed by Borovikov [14]. Extremity points then correspond to the waves diffracted by the edge endpoints and stationary phase points to waves diffracted from the edge itself. This difference highlights the Huygens spherical waves emitted by endpoints which interfere with each other [see Fig. 3(b) and (d)] and render the Huygens field continuous at endpoints shadow boundaries contrary to GTD. In Fig. 3(b) and (d), the difference between GTD and Huygens (or ITD) increases near the edge, $y \sim 0$ mm. That does not matter because near the edge, neither GTD nor Huygens (nor ITD) provide a valid result since they are far-field approximations. In the edge near field, Huygens is closer to GTD than ITD and in far field Huygens and ITD are similar. In near field, the ITD coefficient given by (24) and depending on the local angle ϕ varies more rapidly than the Huygens one from a diffraction point to another, and the summation of secondary sources is more destructive. These observations are more pronounced for the mode-converted transversal diffracted wave shown in Fig. 4.

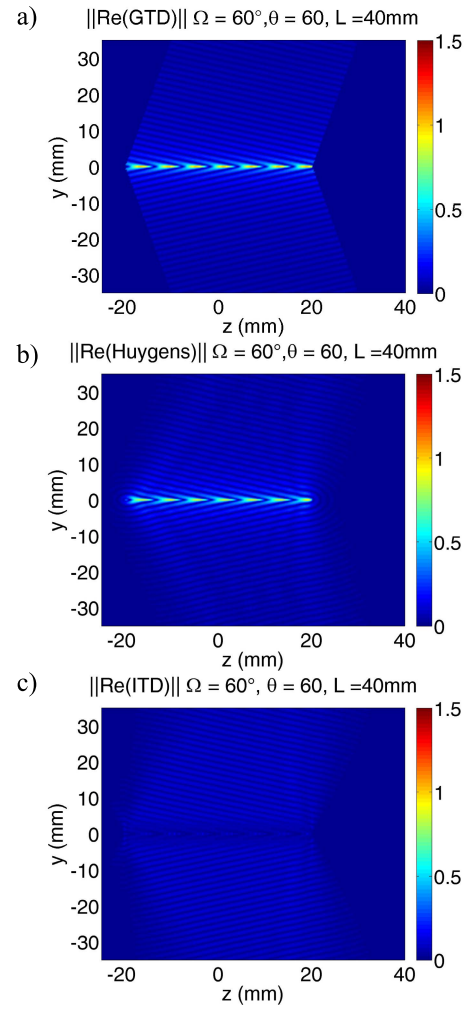

Fig. 4. Results in the configuration of Fig. 3 for the transversal diffracted wave: (a), (b), and (c) with the same meaning as shown in Fig. 3.

Echoes from the endpoints contributions obtained with ITD and Huygens models are not exact since they still rely on canonical GTD solutions (infinite half-plane or wedge). But these incremental methods produce a spatially continuous field and, consequently, a more physical representation than GTD one's.

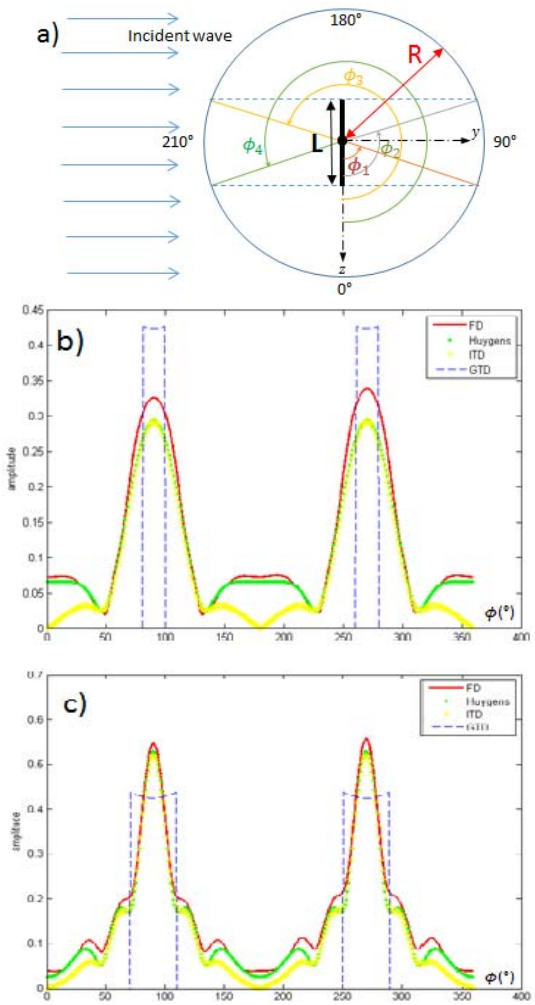

Fig. 5. (a) Edge of length L impinged by an incident longitudinal plane wave. Longitudinal edge diffracted field simulated by different models: (b) $L = 10$ mm and (c) $L = 20$ mm.

It has been numerically checked that as the edge length increases, the Huygens and ITD models both converge to GTD.

The second test is a comparison between GTD, Huygens, ITD, and a finite difference (FD) numerical model [15]. An edge of length L [see Fig. 5(a)] is impinged by an incident longitudinal plane wave. The amplitude (absolute value) of the longitudinal edge diffracted field is plotted for two flaw lengths L versus the observation angle ϕ of observation points located in the plane (e'_y, e'_z) at a distance $R = 30$ mm of five wavelengths from the flaw center. Since this observation plane is in the shadow boundary of the incident $(\theta = \theta_\alpha)$ or reflected $(\theta = 2\pi - \theta_\alpha)$ fields, the analytical models are all combined with UTD [16]: the UTD diffraction coefficient is then finite contrary to the GTD one. As shown in Figs. 3 and 4, the GTD diffracted field is discontinuous at the shadow boundaries [angles $\phi_1, \ldots, \phi_4$ in Fig. 5(a)] emanating from the edge endpoints. ITD and Huygens methods give generally accurate and similar results for observation points for which there exists a GTD diffraction point on the edge $(\phi_1 < \phi < \phi_2)$ and $(\phi_3 < \phi < \phi_4)$ and even around these regions. Huygens has a more physical behavior than ITD for small edge lengths for regions surrounding $\phi = 0$ and $\phi = 180°$ (where ITD vanishes due to destructive interferences as shown also in Figs. 3(c) and 4(c) for $y = 0$).

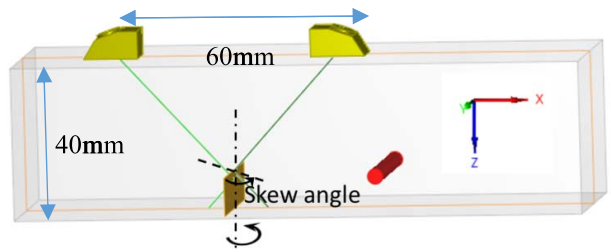

Fig. 6. TOFD inspection used for experimental validation.

C. Experimental Validation

The echoes diffracted by the top tip of a 40-mm-long and 10-mm-high planar notch breaking the back wall of a ferritic steel component have been simulated by the two previous incremental methods and compared to both experimental and numerical results. This comparison briefly presented in [17, Sec. II] is reproduced here to make this paper self-consistent since the theory of incremental methods is completely detailed here[1]; the results simulated by a Huygens/2.5-D GTD model and by a hybrid numerical model are shown here in addition. The objective of this experimental validation is to evaluate the ability of the developed incremental models to simulate the echo amplitude of a defect edge of finite extent.

The diffraction echoes have been measured in a time-of-flight diffraction (TOFD) contact configuration (see Fig. 6) using two 6.35 mm diameter, single element, Plexiglas wedge-type transducers emitting compressional P-waves at 45° incidence and 2.25 MHz. The flaw skew angle (angle between the top edge of the notch and **Y**-axis, see Fig. 6) has been varied from 0° to 70° by rotating the specimen around the **Z**-axis. S-waves are generated in the specimen but the main and first arrival echo from the specimen bulk is due to incident P-wave->scattered P-wave diffraction from the top crack edge. To compute the ultrasonic response of flaws, we have used a reciprocity-based measurement model whose principles and abilities are described in more detail in [18]. In order to avoid modeling of the pulser, cabling, electroacoustic transduction, and electronics at emission/reception, this model requires as input the experimental signal obtained by a calibration measurement on a reference flaw. A side-drilled hole of 2 mm diameter and 40 mm length (in red shown in Fig. 6) has been used for calibration. Our first measurement model [18] applied plane-wave approximations to the ultrasonic fields at each flaw mesh point in order to calculate diffraction coefficients. It yields satisfying results in most usual configurations but can lead to inaccuracies in unfavorable cases, such as for wide probe apertures, outside of the focal region, or for beam-splitting or distortion due to irregular geometries.

A new ray-based model [19] describes the ultrasonic field as a sum of rays emanating from meshed points of the transducer surface and applies the plane-wave approximation to each ray

[1]Only the main results are presented in [17] (reusing portions from [17] in other works are allowed). This paper is cited in [17] under the submitted reference [10] to refer to the theory of the incremental models.

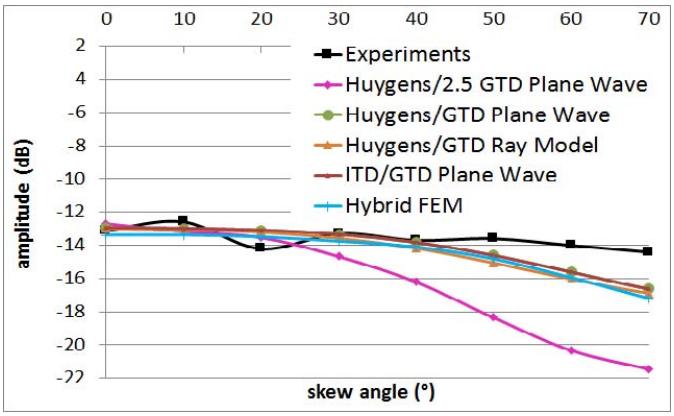

Fig. 7. Echo amplitude diffracted by the top tip.

instead of the entire mean field. It can significantly improve the accuracy of echo computations since the GTD diffraction coefficient is calculated at each mesh flaw contour point for each pair of incident and diffracted rays instead of being calculated only once. In Fig. 7, the maximal amplitude of the P->P echo signal is plotted for both experimental and simulated results. In the current configuration, plane-wave approximation and the ray-based model lead to quasi-identical results since the flaw is far from the probes and the maximal flaw echo amplitude is obtained for the flaw edge location on the probes focal axis. The ray-based model results are slightly closer to those of a hybrid finite elements method model [20] (mixing a ray model for beam calculation and spectral finite elements for flaw scattering modeling).

The Huygens/GTD and ITD/GTD results are similar and close to experiments even for large skews with a maximal difference of 2 dB, which is of order of measurement errors [21]. Huygens/2.5-D GTD model breaks down for skew angles greater than 30°. Therefore, the experimental validation of both ITD and Huygens methods in a 3-D configuration and with a finite-size flaw has been successful.

IV. Conclusion

Two incremental methods have been proposed for use in elastodynamics to predict diffraction from edges of a finite length. Both methods are based on the edge integral approach. For the plane-wave incident on a half-plane both methods reproduce the canonical GTD solution, but unlike the latter they lead to a field which is spatially continuous notably at the shadow boundaries due to edge endpoints. The methods have been tested numerically and validated against experiments for a back wall planar crack. Such methods can be combined with the recently developed elastodynamic corrections to GTD, which are valid in the vicinity of shadow boundaries, the PTD [12] and the UTD [16] or in the vicinity of critical angles [22].

Appendix

Let us show how to evaluate the double integral (12). Denoting it by I it can be written as

$$I = \int_{\Gamma}\int_{C_\xi} \boldsymbol{A}(\lambda,\xi)e^{-s' f(\lambda,\xi)} d\lambda d\xi \tag{27}$$

with

$$\boldsymbol{A}(\lambda,\xi) = \frac{i(\kappa_\beta k_\alpha)}{4\pi^2} u^\alpha(Q_l) q_\beta(\xi)\Psi_\beta(\lambda,\xi,\theta_\alpha) \times \sin\lambda \sin\xi \boldsymbol{d_\beta}(\xi,\lambda) \tag{28}$$

and

$$f(\lambda,\xi) = -i\left[\sin\phi\cos(\lambda-\bar\theta)\left(k_\beta^2 - k_\alpha^2\cos^2\xi\right)^{\frac{1}{2}} + k_\alpha\cos\phi\cos\xi\right] \tag{29}$$

where (13) was used. Integral I can be approximated using the steepest descent method [14] to give

$$I \sim \frac{2\pi}{s'}\frac{A(\lambda_s,\xi_s)}{\sqrt{\det H(\lambda_s,\xi_s)}} e^{-s' f(\lambda_s,\xi_s)} \tag{30}$$

where H is the Hessian matrix. All the functions above are evaluated at the phase stationary point at which we have

$$0 = \partial_\lambda f = i\left[\sin\phi\sin(\lambda-\bar\theta)\left(k_\beta^2 - k_\alpha^2\cos^2\xi\right)^{\frac{1}{2}}\right] \tag{31}$$

$$0 = \partial_\xi f = -i\left[k_\alpha^2\sin\phi\cos(\lambda-\bar\theta)\sin\xi \times \cos\xi\left(k_\beta^2 - k_\alpha^2\cos^2\xi\right)^{-\frac{1}{2}} - k_\alpha\cos\phi\sin\xi\right]. \tag{32}$$

Therefore, the stationary point is $\lambda_s = \bar\theta, \xi_s = 0$ or

$$\cos\xi_s = \frac{k_\beta}{k_\alpha}\cos\phi \tag{33}$$

and according to (16), $\xi_s = \Omega_\alpha(\phi)$. We have also

$$\partial^2_{\lambda\lambda} f = i\left[\sin\phi\cos(\lambda-\bar\theta)\left(k_\beta^2 - k_\alpha^2\cos^2\xi\right)^{\frac{1}{2}}\right] \tag{34}$$

$$i\partial^2_{\xi\xi} f = k_\alpha^2\sin\phi\cos(\lambda-\bar\theta)\left(k_\beta^2 - k_\alpha^2\cos^2\xi\right)^{-\frac{1}{2}} \times \left[\cos^2\xi - \sin^2\xi - \frac{k_\alpha^2\sin^2\xi\cos^2\xi}{k_\beta^2 - k_\alpha^2\cos^2\xi}\right] - k_\alpha\cos\phi\cos\xi \tag{35}$$

$$\partial^2_{\lambda\xi} f = \partial^2_{\xi\lambda}(g) = i\left[k_\alpha^2\sin\phi\sin(\lambda-\bar\theta)\sin\xi \times \cos\xi\left(k_\beta^2 - k_\alpha^2\cos^2\xi\right)^{-\frac{1}{2}}\right]. \tag{36}$$

Finally, at the diffraction point (λ_s,ξ_s)

$$\partial^2_{\lambda\lambda} f|_{(\lambda_s,\xi_s)} = ik_\beta\sin^2\phi \tag{37}$$

$$\partial^2_{\xi\xi} f|_{(\lambda_s,\xi_s)} = i\frac{k_\alpha^2 - k_\beta^2\cos^2\phi}{k_\beta\sin^2\phi} \tag{38}$$

$$\partial^2_{\lambda\xi}(g)|_{(\lambda_s,\xi_s)} = 0. \tag{39}$$

Using (39)–(41), the Hessian matrix at the stationary point is

$$H(\lambda_s,\xi_s) = \begin{bmatrix} ik_\beta\sin^2\phi & 0 \\ 0 & i\dfrac{k_\alpha^2 - k_\beta^2\cos^2\phi}{k_\beta\sin^2\phi} \end{bmatrix} \tag{40}$$

and

$$\det[H(\lambda_s,\xi_s)] = -k_\alpha^2\sin^2\Omega_\alpha(\phi). \tag{41}$$

Since

$$f(\lambda_s,\xi_s) = -ik_\beta \tag{42}$$

$$\boldsymbol{A}(\lambda_s,\xi_s) = \frac{i(\kappa_\beta k_\alpha)}{4\pi^2} u^\alpha(Q_l) q_\beta(\Omega_\alpha(\phi))\Psi_\beta(\bar\theta,\Omega_\alpha(\phi),\theta_\alpha) \times |\sin\theta|\sin\Omega_\alpha(\phi)\boldsymbol{d_\beta}(\phi,\theta) \tag{43}$$

substituting the above expressions into (3), we get

$$I \sim \frac{1}{2\pi}\frac{e^{ik_\beta s'}}{s'}\sin\phi u^\alpha(Q_l)k_\beta^2\Psi_\beta(\bar{\theta},\Omega_\alpha(\phi),\theta_\alpha) \times |\sin\theta|\boldsymbol{d_\beta}(\phi,\theta) \quad (44)$$

and according to (8)

$$I \sim \frac{\sin\phi}{\sqrt{2i\pi}}u^\alpha(Q_l)\frac{e^{ik_\beta s'}}{s'}D_\beta^\alpha(\Omega_\alpha(\phi),\theta_\alpha,\theta)\boldsymbol{d_\beta}(\phi,\theta). \quad (45)$$

References

[1] J. B. Keller, "Geometrical theory of diffraction," *J. Opt. Soc. Amer.*, vol. 52, no. 2, pp. 116–130, 1962.

[2] J. D. Achenbach, A. K. Gautesen, and H. McMaken, *Ray Methods for Waves in Elastic Solids*. New York, NY, USA: Pitman, 1982.

[3] D. Bouche, F. Molinet, and R. Mittra, *Asymptotic Methods in Electromagnetics*. Berlin, Germany: Springer, 1997.

[4] R. Tiberio and S. Maci, "An incremental theory of diffraction: Scalar formulation," *IEEE Trans. Antennas Propag.*, vol. 42, no. 5, pp. 600–612, May 1994.

[5] R. Tiberio, S. Maci, and A. Toccafondi, "An incremental theory of diffraction: Electromagnetic formulation," *IEEE Trans. Antennas Propag.*, vol. 43, no. 1, pp. 87–96, Jan. 1995.

[6] R. Tiberio, A. Toccafondi, A. Polemi, and S. Maci, "Incremental theory of diffraction: A new-improved formulation," *IEEE Trans. Antennas Propag.*, vol. 52, no. 9, pp. 2234–2243, Sep. 2004.

[7] A. D. Yaghjian, "Incremental length diffraction coefficients for arbitrary cylindrical scatterers," *IEEE Trans. Antennas Propag.*, vol. 49, no. 7, pp. 1025–1032, Jul. 2001.

[8] A. Michaeli, "Elimination of infinities in equivalent edge currents, Part II: Physical optics components," *IEEE Trans. Antennas Propag.*, vol. AP-34, no. 8, pp. 1034–1037, Aug. 1986.

[9] R. G. Kouyoumjian and P. H. Pathak, "A uniform geometrical theory of diffraction for an edge in a perfectly conducting surface," *Proc. IEEE*, vol. 62, no. 11, pp. 1448–1461, Nov. 1974.

[10] A. J. Dawson, J. E. Michaels, J. W. Kummer, and T. E. Michaels, "Quantification of shear wave scattering from far-surface defects via ultrasonic wavefield measurements," *IEEE Trans. Ultrason., Ferroelectr., Freq. Control*, vol. 64, no. 3, pp. 590–601, Mar. 2017.

[11] L. J. Fradkin and R. Stacey, "The high-frequency description of scatter of a plane compressional wave by an elliptic crack," *Ultrasonics*, vol. 50, nos. 4–5, pp. 529–538, 2010.

[12] V. Zernov, L. Fradkin, and M. Darmon, "A refinement of the kirchhoff approximation to the scattered elastic fields," *Ultrasonics*, vol. 52, no. 7, pp. 830–835, 2012.

[13] A. K. Djakou, "Modeling of diffraction effects for specimen echoes simulations in ultrasonic non-destructive testing (NDT)," Ph.D. dissertation, École Doctorale SPIGA, Univ. du Maine, Le Mans, France, 2016.

[14] V. A. Borovikov, *Uniform Stationary Phase Method*. London, U.K.: IEE, 1994.

[15] E. Bossy, M. Talmant, and P. Laugier, "Three-dimensional simulations of ultrasonic axial transmission velocity measurement on cortical bone models," *J. Acoust. Soc. Amer.*, vol. 115, no. 5, pp. 2314–2324, Apr. 2004.

[16] A. K. Djakou, M. Darmon, L. Fradkin, and C. Potel, "The uniform geometrical theory of diffraction for elastodynamics: Plane wave scattering from a half-plane," *J. Acoust. Soc. Amer.*, vol. 138, no. 5, pp. 3272–3281, Nov. 2015.

[17] A. K. Djakou, M. Darmon, and C. Potel, "Elastodynamic models for extending GTD to penumbra and finite size scatterers," *Phys. Procedia*, vol. 70, pp. 545–549, 2015. [Online]. Available: https://www.sciencedirect.com/science/article/pii/S1875389215007543

[18] M. Darmon and S. Chatillon, "Main features of a complete ultrasonic measurement model - Formal aspects of modeling of both transducers radiation and ultrasonic flaws responses," *Open J. Acoust.*, vol. 3, pp. 43–53, Sep. 2013.

[19] V. Dorval, N. Leymarie, and S. Chatillon, "Improved semi-analytical simulation of UT inspections using a ray-based decomposition of the incident fields," in *Proc. AIP Conf.*, vol. 1706, 2016, Art. no. 070002.

[20] A. Imperiale, S. Chatillon, M. Darmon, N. Leymarie, and E. Demaldent, "UT simulation using a fully automated 3D hybrid model: Application to planar backwall breaking defects inspection," in *Proc. AIP Conf.*, Apr. 2018, vol. 1949, no. 1, Art. no. 050004.

[21] R. Raillon-Picot, G. Toullelan, M. Darmon, and S. Lonne, "Experimental study for the validation of CIVA predictions in TOFD inspections," in *Proc. 10th Int. Conf. NDE Relation Struct. Integrity Nucl. Pressurized Compon.*, 2013. [Online]. Available: https://www.ndt.net/article/jrc-nde2013/papers/660.pdf

[22] L. J. Fradkin, M. Darmon, S. Chatillon, and P. Calmon, "A semi-numerical model for near-critical angle scattering," *J. Acoust. Soc. Amer.*, vol. 139, no. 1, pp. 141–150, Jan. 2016.

Michel Darmon received the French Engineering degree from ESPCI ParisTech, Paris, France, in 1999, the Ph.D. degree in physical acoustics from the University of Paris VII, Paris, in 2002, and the Habilitation degree from the University of Paris-Sud XI, Orsay, France, in 2015.

His research on modeling the ultrasonic response of solid inclusions was carried out at CEA/LIST, Gif-Sur-Yvette, France, and ArcelorMittal, Maizières-lès-Metz, France. He is currently an expert of the French Atomic Energy Commission (CEA/LIST). His research activity is in ultrasonic modeling notably in flaws scattering and wave propagation in complex media.

Audrey Kamta Djakou received the French Engineering degree from ENSEIRB-MATMECA, Bordeaux, France, in 2013, and the Ph.D. degree in acoustics from the University of Maine, Le Mans, France, in 2016.

Her Ph.D. research carried out at CEA/LIST, Gif-Sur-Yvette, France, is about nondestructive testing (NDT) simulation and notably waves' diffraction.

Samar Chehade received the French Engineering degree from ENSTA ParisTech, Palaiseau, France, in 2016. She is currently pursuing the Ph.D. degree in acoustics with the Paris-Sud University, Orsay, France.

Her research carried out at CEA/LIST is about nondestructive testing (NDT) simulation and notably acoustic and elastic waves' diffraction.

Catherine Potel received the Ph.D. degree in mechanical engineering from the University of Technology of Compiègne (UTC), Compiègne, France, in 1994.

She was a Lecturer with the University of Amiens, Amiens, France, from 1996 to 2001. She has been a Professor of physical acoustics and of mechanics with the University of Le Mans, Le Mans, France, in the Laboratoire d'Acoustique de l'Université du Maine since 2001. Her research is in ultrasonics for nondestructive evaluation and materials characterization, with a special interest in propagation in anisotropic multilayered media such as composites and in rough plates.

Larissa Fradkin received the Ph.D. degree in applied mathematics from the Victoria University of Wellington, Wellington, New Zealand, in 1977.

From 1977 to 1984, she was a Research Scientist with the N.Z. Department of Scientific and Industrial Research. From 1985 to 1993, she was a Research Associate with the Department of Applied Mathematics and Theoretical Physics, University of Cambridge, Cambridge, U.K. From 1993 to 2009, she was a Senior Lecturer, a Reader, and a Professor of electrical engineering with London South Bank University, London, U.K. Since 2009, she has been running a micro-company, Sound Mathematics Ltd., in Cambridge. Her research interests include mathematical modeling of ultrasonic nondestructive testing (NDT) (notably high-frequency phenomena in elastodynamics).